

Patterning Superconductivity in a Topological Insulator

Jerome T. Mlack,^{†,‡,§,ID} Atikur Rahman,[†] Gopinath Danda,^{‡,§,ID} Natalia Drichko,[†] Sarah Friedensen,[‡] Marija Drndić,[‡] and Nina Marković^{*,†,§,ID}

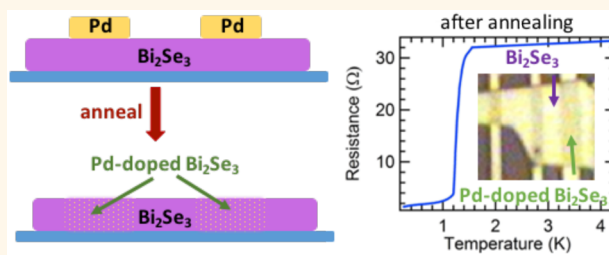
[†]Department of Physics and Astronomy, Johns Hopkins University, Baltimore, Maryland 21218, United States

[‡]Department of Physics and Astronomy and [§]Department of Electrical and Systems Engineering, University of Pennsylvania, Philadelphia, Pennsylvania 19104, United States

^{*}Department of Physics and Astronomy, Goucher College, Baltimore, Maryland 21204, United States

ABSTRACT: Topologically protected states in combination with superconductivity hold great promise for quantum computing applications, but the progress on electrical transport measurements in such systems has been impeded by the difficulty of fabricating devices with reliable electrical contacts. We find that superconductivity can be patterned directly into Bi_2Se_3 nanostructures by local doping with palladium. Superconducting regions are defined by depositing palladium on top of the nanostructures using electron beam lithography followed by *in situ* annealing. Electrical transport measurements at low temperatures show either partial or full superconducting transition, depending on the doping conditions. Structural characterization techniques indicate that palladium remains localized in the targeted areas, making it possible to pattern superconducting circuits of arbitrary shapes in this topological material.

KEYWORDS: topological insulators, patterning, superconductivity, electron transport, transmission electron microscopy, Raman spectroscopy



Topological superconductors are predicted to host Majorana fermions,^{1,2} which may be used as building blocks for fault-tolerant quantum computing.^{3,4} Whereas some evidence of topological superconductivity has been found in doped bulk topological insulators^{5–11} and Majorana fermions have been reported in one-dimensional systems in proximity to superconductors,^{12–15} one of the remaining challenges is to find a convenient experimental platform for realizing circuits that would allow a pairwise exchange of Majorana fermions known as braiding.⁴

Bi_2Se_3 is a widely studied topological insulator¹⁶ that is known to become superconducting upon doping with copper or other metallic elements.^{5,8,10} The bulk Cu-doped Bi_2Se_3 was predicted to have topological properties,¹⁷ which have been reported in some experiments,^{9–11} whereas others indicated conventional superconductivity.^{18,19} It has been shown that the stability and the properties of this material depend critically on growth and quenching conditions.²⁰ An alternative to bulk doping is to induce superconductivity on the surface of Bi_2Se_3 by proximity to a conventional superconductor.^{21–24} Whereas both the bulk-doped and proximity-coupled systems are convenient platforms for studying topological superconductivity by spectroscopic methods, harnessing their topological properties will require transport measurements, which remain

to be a challenge due to the difficult device architecture and poor electrical contacts.

Some of these issues could be effectively resolved by combining the above approaches in order to create native superconducting and normal regions in desired patterns within the crystal of a topological insulator. Here, we show that superconductivity can be patterned directly into a topological insulator Bi_2Se_3 by doping selected regions with palladium (Pd), using electron beam lithography and *in situ* annealing. Electrical transport measurements at low temperatures show superconducting transitions in the doped regions, whereas structural characterization techniques indicate that Pd remains localized in the targeted areas. By providing superconductivity in desired locations with clean interfaces, this will lend itself to patterning devices and enable the transport measurements that are needed for applications.

RESULTS AND DISCUSSION

Bi_2Se_3 nanocrystals of thickness between 70 and 100 nm were mechanically exfoliated onto Si substrates. Pd leads were patterned and deposited onto the nanocrystals using standard

Received: March 4, 2017

Accepted: May 23, 2017

Published: May 23, 2017



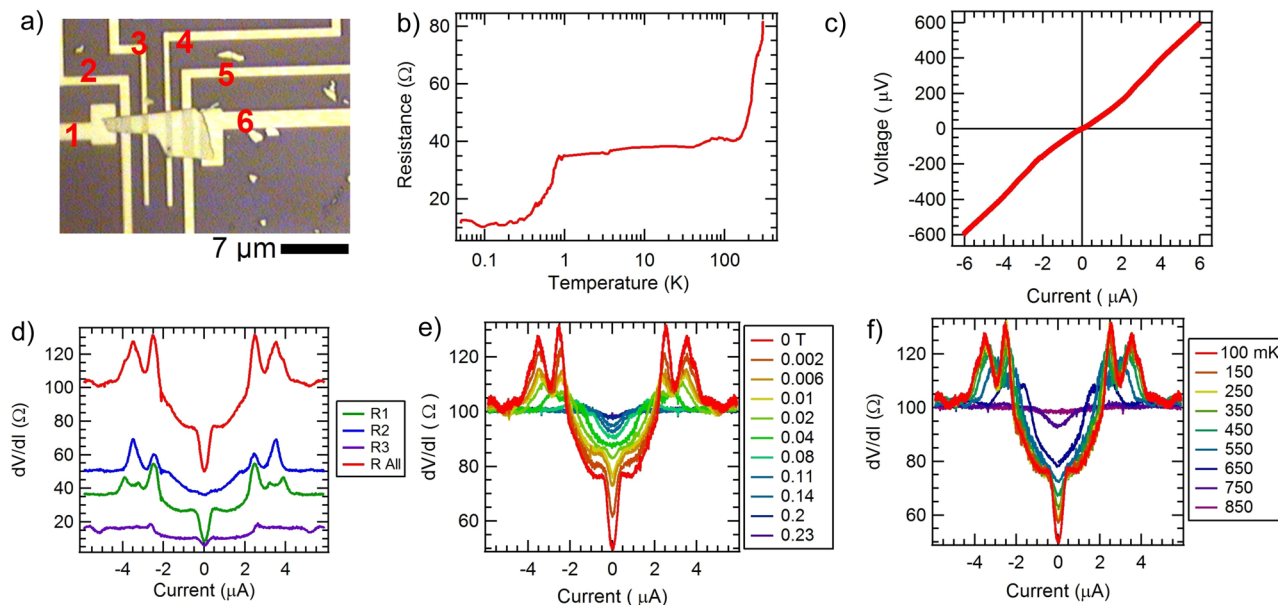


Figure 1. Electrical measurements of a Pd-doped Bi_2Se_3 device after annealing. (a) Optical microscope image of a sample after annealing under flowing Ar gas at 220 °C for 1 h. The irregular shape in the center is an exfoliated Bi_2Se_3 flake, and the Pd leads are marked by numbers 1–6. The parts of the Bi_2Se_3 flake that had been covered with 90 nm of Pd appear darker in the image. (b) Four-probe resistance as a function of temperature with current sourced across leads 1 and 6 and voltage measured across leads 2 and 3. A transition to a lower resistance state is observed around 800 mK. (c) Four-probe V - I curve with current sourced from leads 1 to 6 and voltage measured across leads 2 and 5. (d) Four-probe differential resistance measurements with current sourced from lead 1 to 6 and voltage measured across leads 2 and 5 (red), leads 2 and 3 (green, region 1), leads 3 and 4 (blue, region 2), and leads 4 and 5 (purple, region 3). All three regions show transitions but at slightly different bias currents. Differential resistance measurements of the whole device, with voltage measured across 2 and 5, are shown as a function of magnetic field (e) and temperature (f). In both sets of data, two primary peaks are observed at 2.5 and 3.5 μA .

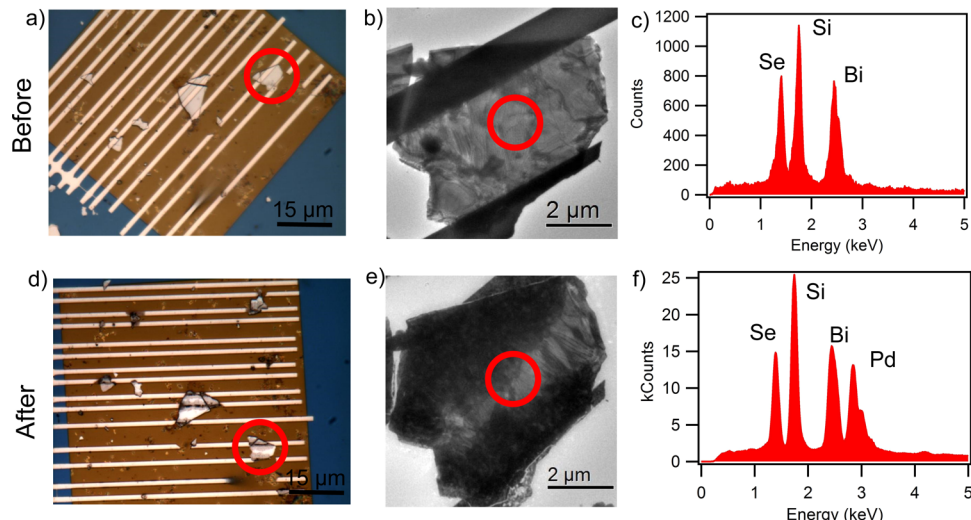


Figure 2. Images and EDS spectra of exfoliated Bi_2Se_3 flakes before and after thermal annealing. (a) Optical image of Bi_2Se_3 flakes exfoliated onto a silicon nitride window and covered with lines of palladium. (b) TEM image of a flake with a palladium line, circled in red in (a). (c) EDS spectra of red circled area in (b) showing composition of Bi_2Se_3 and signal from the silicon nitride window. (d) Optical image of flakes shown in (a) after thermal annealing for 1 h at 295 °C under argon gas flowing at 200 sccm. (e) TEM image of a flake, circled in red in (d), post-annealing. (f) EDS spectra, from location circled in red in (e), post-annealing, indicating that palladium has entered into the flake.

electron beam and optical lithography methods. Bi_2Se_3 devices with Pd leads were metallic down to 0.25 K, and neither pure palladium nor Bi_2Se_3 is superconducting on their own. The devices were annealed at a temperature between 200 and 300 °C. An optical image of a device that was annealed at 220 °C is shown in Figure 1a. After being annealed, the 100 nm thick Pd leads are no longer visible by atomic force microscope measurements on top of Bi_2Se_3 , while still showing the 100

nm thickness everywhere else. We show below that the Pd is absorbed by the Bi_2Se_3 crystal during annealing. A second layer of palladium leads was added over the doped areas in order to ensure good contact for electrical measurements. After being annealed, the devices showed a superconducting transition around 0.8 K, as shown in Figure 1.

A four-probe measurement of the resistance as a function of temperature between leads 2 and 3 of Figure 1a is shown in

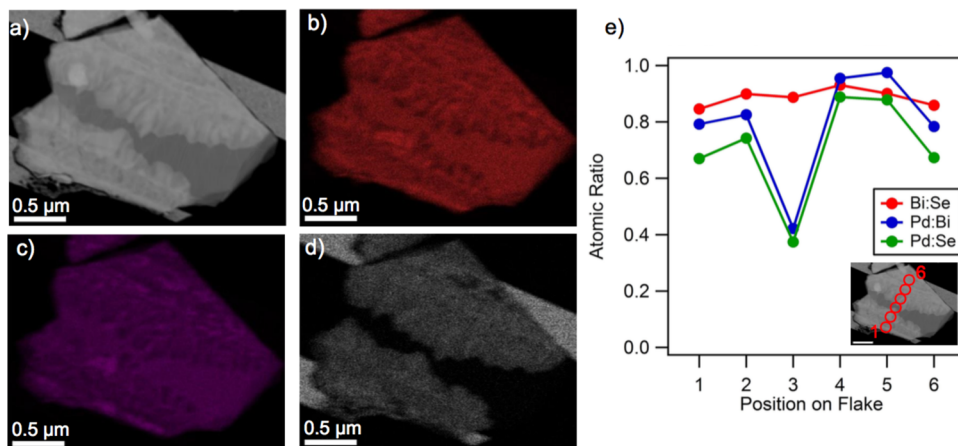


Figure 3. Elemental EDS maps of an annealed Bi_2Se_3 flake depicted in **Figure 2e**, atomic ratios across the cross section of the flake, and selected area diffraction images from several positions on the flake. (a) Counts per second map of the annealed flake. (b) Mapping of bismuth. (c) Mapping of selenium. (d) Mapping of palladium. (e) Atomic ratios of Bi/Se (red), Pd/Bi (blue), and Pd/Se (green) at several locations along the cross section of the flake, as depicted in the inset, starting with position 1 in the lower left-hand corner to position 6 in the upper right.

Figure 1b. A transition to a low-resistance state is observed at 0.8 K. The resistance does not drop to zero, but the nonlinear current–voltage characteristics indicate that the portion of the sample is superconducting. As we will show below, the resistance below the transition is caused by a section of the crystal between the leads, which remains undoped. The current–voltage measurement across the entire device, with current sourced between leads 1 and 6 and voltage measured across leads 2 and 5, is shown in **Figure 1c**. The nonlinear behavior above 2 μA is emphasized in the differential conductance, measured on different regions of the device, shown in **Figure 1d**.

Temperature and magnetic field dependence of the differential resistance across the entire device is shown in **Figure 1e,f**, respectively. As either the temperature or magnetic field is increased, the dip in resistivity at low currents gradually disappears, which is typical for superconducting samples with a critical field of about 0.2 T. In both sets of data, two primary peaks are observed at 2.5 and 3.5 μA . A similar behavior of dV/dI has been reported previously in Bi_2Se_3 samples in which superconductivity was induced on the surface by proximity to a conventional superconductor.^{22,23} In our samples, Pd leads are not superconducting, so the superconductivity must be due to the annealing step.

In order to investigate what happens to the Pd during the annealing process, samples were imaged using a transmission electron microscope (TEM) before and after annealing, as shown in **Figure 2** and **Figure 3**. Bi_2Se_3 flakes were exfoliated onto a 100 nm thick silicon nitride TEM window with 90 nm thick palladium lines deposited across the flakes. **Figure 2a** shows an optical microscope image of a sample before annealing. A representative flake, circled in red in **Figure 2a**, is shown in the TEM image in **Figure 2b**. **Figure 2c** is the energy-dispersive X-ray (EDS) spectrum for the area of the flake circled in red in **Figure 2b**. The EDS spectrum indicates that the central region of the flake is pure Bi_2Se_3 with a background Si signal from the substrate.

The same sample is shown in **Figure 2d–f** after annealing at 290 °C. In the optical image of **Figure 2d**, the exfoliated flakes that were in contact with Pd show a clear change in color in the vicinity of the Pd lines. The TEM image in **Figure 2e** shows

that the flake from **Figure 2b** has undergone a drastic change after annealing. The flake is overall less transparent and the contact to the Pd lines has disappeared, indicating that the Bi_2Se_3 flake has absorbed the palladium. Further evidence that the Pd has spread into the flake is provided by the EDS spectrum from the same region as **Figure 2c**, which now includes a peak indicating the presence of Pd along with the original Bi, Se, and Si peaks.

In order to better understand the dynamics and the extent of Pd migration in the Bi_2Se_3 flake, EDS map of the flake shown in **Figure 2** was acquired after annealing, as shown in **Figure 3**. The elemental spatial maps show that Bi (**Figure 3b**) and Se (**Figure 3c**) peaks were present across the entire flake, and the Pd (**Figure 3d**) extended only up to a certain length into the flake from the leads, leaving the central region an unaltered Bi_2Se_3 . The weaker peak intensity of Pd at the lead–flake–substrate interface compared to lead–substrate interface and the uniform atomic ratio of Pd inside the flake suggest that the Pd atoms move from the leads into the flake during annealing until a steady-state concentration is reached.

In **Figure 3e**, the atomic ratios of Bi/Se, Pd/Bi, and Pd/Se were calculated along a line profile (point scan area = 0.04 μm^2), as shown in **Figure 3e**. The ratios of Pd/Bi and Pd/Se were both seen to have a valley in the central region as expected due to the absence of Pd, consistent with the EDS Pd map. It was seen that the Bi/Se atomic ratio remained approximately constant throughout at a value slightly greater than 0.7 or 2:3; that is, the Se concentration was lower than expected, indicating that some loss occurred as a result of the annealing process. While Bi_2Se_3 typically shows metallic properties in the bulk due to Se vacancies, these properties can be controlled by growth methods,²⁵ chemical doping,²⁶ or electrostatic doping.²⁶

To further investigate the motion of Pd inside Bi_2Se_3 , electron diffraction was studied in three different regions, specified in **Figure 4a**. Region 1 is an unaltered Bi_2Se_3 region, whereas regions 2 and 3 did not contain Pd before annealing. The diffraction in region 1 (**Figure 4b**) shows the normal hexagonal Bi_2Se_3 radial pattern for the [11̄20] direction, with a calculated lattice parameter value of $a = 0.413 \text{ nm}$.

A distorted polycrystalline lattice structure was obtained for regions 2 and 3, shown in **Figure 4c,d**, respectively. The

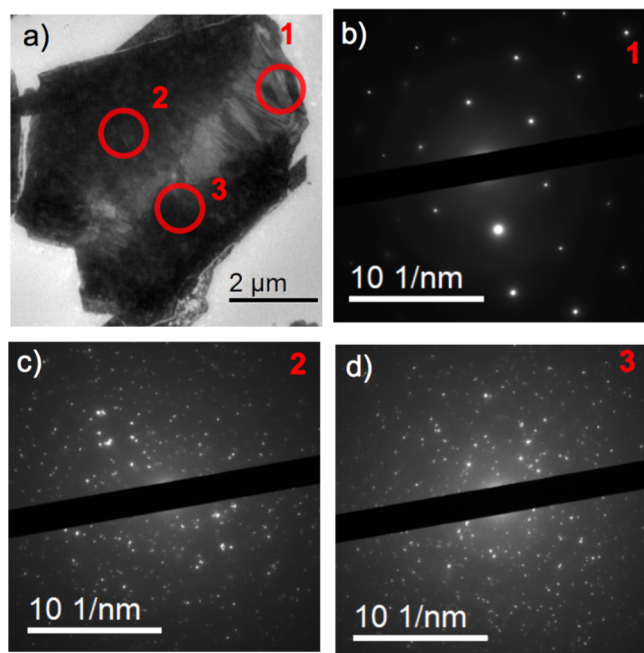


Figure 4. (a) Image of a flake with regions chosen for diffraction identified. (b) Selected area electron diffraction from region 1 in (a), showing a hexagonal crystal lattice with radial pattern corresponding to $[1\bar{1}\bar{2}0]$ and lattice constant $a = 0.413$ nm. (c) Selected area electron diffraction from region 2 in (a), showing a polycrystalline pattern. (d) Selected area electron diffraction from region 3 in (a), showing a polycrystalline pattern.

constant Bi/Se atomic ratio and the presence of a polycrystalline diffraction pattern in regions 2 and 3 suggest that Pd is disrupting the host crystal structure without altering the relative concentration of Bi and Se atoms. Further in-depth material characterization is required for better understanding and tuning the Pd migration in Bi_2Se_3 .

Overall, the TEM analysis of the annealed flake shows that the Pd is absorbed by the Bi_2Se_3 flake during the annealing process and that the absorption occurs uniformly with a leading edge across the flake. Although superconductivity has been reported before in several compounds containing Pd and Bi or

Se,^{27–29} transport data and the TEM analysis do not show that such compounds are forming in our samples.

By comparing optical images and EDS data, we see that the regions penetrated by Pd appear gray on the optical images, providing a simple way to optically locate the Pd. Comparing samples annealed at different temperatures, we find that the extent of the Pd spreading can be controlled by the annealing temperature. At lower annealing temperatures, Pd is absorbed only in the targeted areas (as in Figure 1 and Figure 5), whereas at higher annealing temperatures, it also spreads away from the targeted areas (as in Figure 3). Additional measurements taken over several weeks indicate that the samples do not degrade with time, and the Pd remains in place.

Further evidence that the Bi_2Se_3 crystal structure remains intact away from the targeted areas is provided by Raman spectroscopy. Figure 5 shows the Raman spectra taken on the Bi_2Se_3 flake about 5 μm away from the Pd line (position 1), on top of the Pd line (position 2), and on the Bi_2Se_3 flake directly adjacent to the Pd line (positions 3 and 4). In the spectra recorded at positions 1, 3, and 4, we observe phonon bands at 73, 132, and 176 cm⁻¹, which is typically found for Bi_2Se_3 .³⁰ The widths of the lines are 5–8 cm⁻¹, which is also typical for bulk Bi_2Se_3 . These results confirm that the crystal structure of the material is unchanged at these positions. We do not observe the Raman bands on top of the Pd line (position 2) because the Pd layer on the surface of the Bi_2Se_3 flake prevents the propagation of the visible excitation light.

CONCLUSIONS

The combination of optical, TEM, EDS, and Raman spectroscopy with electrical measurements shows that Pd is absorbed by the Bi_2Se_3 crystal only in the targeted areas, allowing us to pattern superconductivity in Bi_2Se_3 . More work is needed to determine the nature of superconductivity in Pd-doped Bi_2Se_3 . Regardless of whether the patterned regions show topological superconductivity in their own right or just provide conventional superconductivity in proximity to topological insulator, the patterning provides a promising platform for building 2D topological devices.

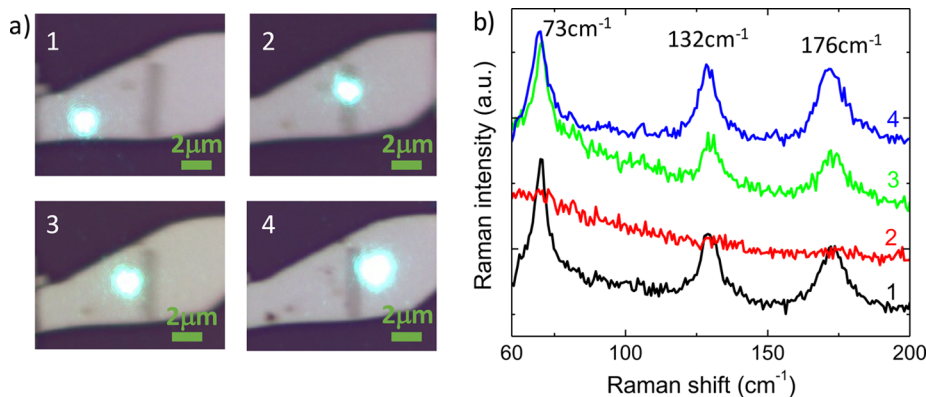


Figure 5. Raman spectroscopy of Pd-doped Bi_2Se_3 flakes after annealing at 200 °C. (a) Optical images of a Bi_2Se_3 flake (light gray) exfoliated onto a silicon oxide substrate (black background). The darker gray vertical line in the center of the flake is a 90 nm thick layer of Pd. The bright spot is the image of the Raman laser probe at positions 1 (away from Pd), 2 (on top of Pd), 3 (directly to the left of the Pd), and 4 (directly to the right of the Pd). (b) Raman scattering spectra at positions 1–4 in the range of Bi_2Se_3 phonons. Spectra from positions 1, 3, and 4 show phonons that are expected for pure Bi_2Se_3 . The spectrum from position 2 shows no bands because the layer of Pd on top of Bi_2Se_3 is not transparent to light with the wavelength of 514 nm.

METHODS

Bi_2Se_3 nanocrystals of thickness between 70 and 100 nm were mechanically exfoliated onto 300 nm SiO_2 on Si substrates. Pd leads were patterned and deposited onto the nanocrystals using standard electron beam and optical lithography methods. The devices were annealed in a quartz tube furnace at a set temperature between 200 and 300 °C while flowing argon gas through the tube at a rate of 200 sccm. The set temperature was maintained for 1 h, after which the tube furnace was turned off and allowed to cool naturally. A second layer of palladium leads was added over the doped areas in order to ensure good contact for electrical measurements. Raman scattering spectra were measured in backscattering geometry using a Horiba Jobin-Yvon T64000 spectrometer equipped with Olympus microscope. The 514.5 nm line of the Ar^+ laser was used for excitation. The laser power was kept below 1 mW to avoid overheating of the sample. The size of the laser probe was about 2 μm in diameter. The spectra were recorded with 2.5 cm^{-1} spectral resolution.

AUTHOR INFORMATION

Corresponding Author

*E-mail: nina.markovic@goucher.edu.

ORCID

Jerome T. Mlack: [0000-0002-2848-2836](https://orcid.org/0000-0002-2848-2836)

Gopinath Danda: [0000-0003-3455-3474](https://orcid.org/0000-0003-3455-3474)

Nina Marković: [0000-0002-3639-9987](https://orcid.org/0000-0002-3639-9987)

Notes

The authors declare no competing financial interest.

ACKNOWLEDGMENTS

This work was supported by the National Science Foundation through Grants DGE-1232825 (J.T.M.), DMR-1507782, and EFRI 2-DARE 1542707. We would like to thank the JHU Raman Spectroscopy Users Center.

REFERENCES

- (1) Fu, L.; Kane, C. L. Superconducting Proximity Effect and Majorana Fermions at the Surface of a Topological Insulator. *Phys. Rev. Lett.* **2008**, *100*, 096407.
- (2) Beenakker, C. W. J. *Annual Review of Condensed Matter Physics*; Langer, J., Ed.; Annual Reviews, 2013; Vol. 4; pp 113–136.
- (3) Kitaev, A. Fault-Tolerant Quantum Computation by Anyons. *Ann. Phys.* **2003**, *303*, 2–30.
- (4) Nayak, C.; Simon, S. H.; Stern, A.; Freedman, M.; Das Sarma, S. Non-Abelian Anyons and Topological Quantum Computation. *Rev. Mod. Phys.* **2008**, *80*, 1083–1159.
- (5) Hor, Y. S.; Williams, A. J.; Checkelsky, J. G.; Roushan, P.; Seo, J.; Xu, Q.; Zandbergen, H. W.; Yazdani, A.; Ong, N. P.; Cava, R. J. Superconductivity in $\text{Cu}_x\text{Bi}_2\text{Se}_3$ and its Implications for Pairing in the Undoped Topological Insulator. *Phys. Rev. Lett.* **2010**, *104*, 057001.
- (6) Hor, Y.; Checkelsky, J.; Qu, D.; Ong, N.; Cava, R. Superconductivity and Non-Metallicity Induced by Doping the Topological Insulators Bi_2Se_3 and Bi_2Te_3 . *J. Phys. Chem. Solids* **2011**, *72*, 572–576.
- (7) Bay, T. V.; Naka, T.; Huang, Y. K.; Luigjes, H.; Golden, M. S.; de Visser, A. Superconductivity in the Doped Topological Insulator $\text{Cu}_x\text{Bi}_2\text{Se}_3$ Under High Pressure. *Phys. Rev. Lett.* **2012**, *108*, 057001.
- (8) Kriener, M.; Segawa, K.; Ren, Z.; Sasaki, S.; Ando, Y. Bulk Superconducting Phase with a Full Energy Gap in the Doped Topological Insulator $\text{Cu}_x\text{Bi}_2\text{Se}_3$. *Phys. Rev. Lett.* **2011**, *106*, 127004.
- (9) Sasaki, S.; Kriener, M.; Segawa, K.; Yada, K.; Tanaka, Y.; Sato, M.; Ando, Y. Topological Superconductivity in $\text{Cu}_x\text{Bi}_2\text{Se}_3$. *Phys. Rev. Lett.* **2011**, *107*, 217001.
- (10) Liu, Z.; Yao, X.; Shao, J.; Zuo, M.; Pi, L.; Tan, S.; Zhang, C.; Zhang, Y. Superconductivity with Topological Surface State in $\text{Sr}_x\text{Bi}_2\text{Se}_3$. *J. Am. Chem. Soc.* **2015**, *137*, 10512–10515.
- (11) Matano, K.; Kriener, M.; Segawa, K.; Ando, Y.; Zheng, G.-q. Spin-Rotation Symmetry Breaking in the Superconducting State of $\text{Cu}_x\text{Bi}_2\text{Se}_3$. *Nat. Phys.* **2016**, *12*, 852–854.
- (12) Mourik, V.; Zuo, K.; Frolov, S. M.; Plissard, S. R.; Bakkers, E. P. A. M.; Kouwenhoven, L. P. Signatures of Majorana Fermions in Hybrid Superconductor-Semiconductor Nanowire Devices. *Science* **2012**, *336*, 1003–1007.
- (13) Das, A.; Ronen, Y.; Most, Y.; Oreg, Y.; Heiblum, M.; Shtrikman, H. Zero-Bias Peaks and Splitting in an Al-InAs Nanowire Topological Superconductor as a Signature of Majorana Fermions. *Nat. Phys.* **2012**, *8*, 887–895.
- (14) Albrecht, S. V.; Higginbotham, A. P.; Madsen, M.; Kuemmeth, F.; Jespersen, T. S.; Nygård, J.; Krogstrup, P.; Marcus, C. M. Exponential Protection of Zero Modes in Majorana Islands. *Nature* **2016**, *531*, 206–209.
- (15) Nadj-Perge, S.; Drozdov, I. K.; Li, J.; Chen, H.; Jeon, S.; Seo, J.; MacDonald, A. H.; Bernevig, B. A.; Yazdani, A. Observation of Majorana Fermions in Ferromagnetic Atomic Chains on a Superconductor. *Science* **2014**, *346*, 602–607.
- (16) Hasan, M. Z.; Kane, C. L. *Colloquium: Topological Insulators*. *Rev. Mod. Phys.* **2010**, *82*, 3045–3067.
- (17) Fu, L.; Berg, E. Odd-Parity Topological Superconductors: Theory and Application to $\text{Cu}_x\text{Bi}_2\text{Se}_3$. *Phys. Rev. Lett.* **2010**, *105*, 097001.
- (18) Levy, N.; Zhang, T.; Ha, J.; Sharifi, F.; Talin, A. A.; Kuk, Y.; Strocio, J. A. Experimental Evidence for *s*-Wave Pairing Symmetry in Superconducting $\text{Cu}_x\text{Bi}_2\text{Se}_3$ Single Crystals Using a Scanning Tunneling Microscope. *Phys. Rev. Lett.* **2013**, *110*, 117001.
- (19) Peng, H.; De, D.; Lv, B.; Wei, F.; Chu, C.-W. Absence of Zero-Energy Surface Bound States in $\text{Cu}_x\text{Bi}_2\text{Se}_3$ Studied via Andreev Reflection Spectroscopy. *Phys. Rev. B: Condens. Matter Mater. Phys.* **2013**, *88*, 024515.
- (20) Schneeloch, J. A.; Zhong, R. D.; Xu, Z. J.; Gu, G. D.; Tranquada, J. M. Dependence of Superconductivity in $\text{Cu}_x\text{Bi}_2\text{Se}_3$ on Quenching Conditions. *Phys. Rev. B: Condens. Matter Mater. Phys.* **2015**, *91*, 144506.
- (21) Koren, G.; Kirzhner, T.; Lahoud, E.; Chashka, K. B.; Kanigel, A. Proximity-Induced Superconductivity in Topological $\text{Bi}_2\text{Te}_2\text{Se}$ and Bi_2Se_3 films: Robust Zero-Energy Bound State Possibly due to Majorana Fermions. *Phys. Rev. B: Condens. Matter Mater. Phys.* **2011**, *84*, 224521.
- (22) Sacépé, B.; Oostinga, J. B.; Li, J.; Ubaldini, A.; Couto, N. J.; Giannini, E.; Morpurgo, A. F. Gate-Tuned Normal and Superconducting Transport at the Surface of a Topological Insulator. *Nat. Commun.* **2011**, *2*, 575.
- (23) Williams, J. R.; Bestwick, A. J.; Gallagher, P.; Hong, S. S.; Cui, Y.; Bleich, A. S.; Analytis, J. G.; Fisher, I. R.; Goldhaber-Gordon, D. Unconventional Josephson Effect in Hybrid Superconductor-Topological Insulator Devices. *Phys. Rev. Lett.* **2012**, *109*, 056803.
- (24) Cho, S.; Dellabetta, B.; Yang, A.; Schneeloch, J.; Xu, Z.; Valla, T.; Gu, G.; Gilbert, M. J.; Mason, N. Symmetry Protected Josephson Supercurrents in Three-Dimensional Topological Insulators. *Nat. Commun.* **2013**, *4*, 1689.
- (25) Brahlek, M.; Bansal, N.; Koiralal, N.; Xu, S.-Y.; Neupane, M.; Liu, C.; Hasan, M. Z.; Oh, S. Topological-Metal to Band-Insulator Transition in $(\text{Bi}_{1-x}\text{In}_x)_2\text{Se}_3$ Thin Films. *Phys. Rev. Lett.* **2012**, *109*, 186403.
- (26) Kim, D.; Syers, P.; Butch, N. P.; Paglione, J.; Fuhrer, M. S. Coherent Topological Transport on the Surface of Bi_2Se_3 . *Nat. Commun.* **2013**, *4*, 2040.
- (27) Takabatake, T.; Ishikawa, M.; Junod, A. Superconducting Properties of the Pd-Se System. *J. Phys. Soc. Jpn.* **1988**, *57*, 2763–2767.
- (28) Sakamoto, T.; Wakushima, M.; Hinatsu, Y.; Matsuhira, K. Transport Properties in Normal-Metal $\text{Bi}_2\text{Pd}_3\text{S}_2$ and Superconducting $\text{Bi}_2\text{Pd}_3\text{Se}_2$. *Phys. Rev. B: Condens. Matter Mater. Phys.* **2008**, *78*, 024509.
- (29) Weihrich, R.; Matar, S.; Anusca, I.; Pielenhofer, F.; Peter, P.; Bachhuber, F.; Eyert, V. Palladium Site Ordering and the Occurrence of Superconductivity in $\text{Bi}_2\text{Pd}_3\text{Se}_{2-x}\text{S}_x$. *J. Solid State Chem.* **2011**, *184*, 797–804.

- (30) Richter, W.; Becker, C. A Raman and Far-Infrared Investigation of Phonons in the Rhombohedral $V_2 - VI_3$ Compounds Bi_2Te_3 , Bi_2Se_3 , Sb_2Te_3 and $Bi_2(Se_{1-x}Te_x)_3$ ($0 < x < 1$), $(Bi_{1-y}Sb_y)_3Te_3$ ($0 < y < 1$). *Phys. Status Solidi B* **1977**, *84*, 619–628.